



1 **An Improved Method Based on VGGNet for Refined Bathymetry**
2 **from Satellite Altimetry: Reducing the Errors Effectively**

3 **Xiaolun Chen¹, Xiaowen Luo^{1,4}, Ziyin Wu^{1,2,3}, Xiaoming Qin³, Jihong Shang¹,**
4 **Mingwei Wang¹, Hongyang Wan¹**

5 ¹Key Laboratory of Submarine Geosciences, Second Institute of Oceanography,
6 Ministry of Natural Resources, Hangzhou, China

7 ²School of Oceanography, Shanghai Jiao Tong University, Shanghai, China

8 ³Ocean College, Zhejiang University, Zhoushan, China

9 ⁴Key Laboratory of Ocean Space Resource Management Technology, Marine Academy
10 of Zhejiang Province, Hangzhou, China

11
12 **Correspondence:** Xiaowen Luo (cdslxw@163.com); Ziyin Wu (zywu@vip.163.com)
13

14 **Abstract.** At present, only approximately 10% of the global seafloor topography has
15 been finely modeled, and the rest are either lacking in data or not accurate enough to
16 meet practical requirements. On the one hand, satellite altimeter has the advantages of
17 large-scale and real-time observation, thus is widely used in the measurement of
18 bathymetry, the core of seafloor topography. However, there is often room for
19 improvement in its precision. On the other hand, multibeam echosounder bathymetric
20 data is highly precise but normally limited to a smaller coverage, which forms a
21 complementary relationship with the bathymetry derived from satellite altimetry. To
22 combine the advantages of satellite altimetry-derived and multibeam sonar-derived
23 bathymetry, we apply deep learning, which is powerful in the field of digital image
24 automation, to perform multibeam sonar-based bathymetry correction for satellite
25 altimetry bathymetry data. Specifically, we modify and improve a pretrained VGGNet
26 neural network model with a depth of 19 layers to train on three sets of bathymetry data
27 from the West Pacific, Southern Ocean, and East Pacific, respectively. Experiments
28 show that the correlation of bathymetry data before and after correction can reach a
29 high level, with the performance of R^2 being as high as 0.81 and the RMSE improved
30 over 19% compared with previous research. We then explore the relationship between
31 R^2 and water depth and conclude that it varies at different depths and thus the terrain
32 specificity was a factor that affects the precision of correction. Finally, we use the
33 difference of water depth before and after the correction to evaluate the correction
34 results, and find that our method can improve by more than 17% compared with
35 previous research. The results show that using the deep learning VGGNet model can
36 better perform the correction of the bathymetry derived from satellite altimetry, thus
37 providing a method for accurate modeling of the seafloor topography.
38



39 1 Introduction

40 Submarine topographic survey is a basic marine surveying and mapping work,
41 whose purpose is to obtain the three-dimensional coordinates of submarine topographic
42 points, including measurement position, water depth, water level, sound speed, attitude,
43 azimuth and other information, the core of which is water depth measurement. Modern
44 multibeam sounding systems began to rise in the 1960s. Fox et al. (1992) conducted a
45 quantitative analysis of the changes in the submarine topography caused by the
46 submarine volcanic eruption based on the multibeam sonar data and the submarine
47 robot's measured images. Wu (2001) put forward the key statistical parameters to attain
48 the seafloor tracking of the multibeam sounding system and established the
49 mathematical model and expert system for real-time tracking of the seafloor terrain.
50 Schimel et al. (2015) analyzed the continuous observation of multibeam data and found
51 that the uncertainty information provided by the multibeam processing algorithm
52 CUBE can be used to better calculate the displacement of the sediment volume. Ma et
53 al. (2006) found that full coverage and high-efficiency multibeam sonar can be
54 combined with side-scan sonar, which has good complementarity when detecting
55 submarine targets, and can improve the accuracy of target recognition. Ji (2017) applied
56 backpropagation (BP) neural network to build a feature database of seabed terrain based
57 on multibeam data to attain automatic classification of seabed terrain complexity. Pike
58 et al. (2019) combined Pleiades multispectral imagery and multibeam data to measure
59 the water depth of two shallow waters in the northeastern Caribbean. Cooper et al. (2021)
60 proposed a method that uses small unmanned aerial vehicle (sUAV) photogrammetry
61 as well as multibeam sonar data to generate a complete bathymetry map of a reservoir.

62 The multibeam sounding method has the advantage of high spatial precision, which
63 enables the underwater sounding mode to achieve a high-quality leap from point to line
64 and from line to surface (Li, 1999). However, with the low efficiency, high cost and
65 long measurement time required, these shortcomings make it difficult to conduct
66 submarine surveys in a wide range of sea areas. Thus, the coverage of shipborne
67 soundings is still very sparse at present. It's estimated that only about 10% of the global
68 sea area is covered with shipborne survey data, and a considerable part of it, especially
69 in the deep ocean areas, consists of analog signals from 1950 to 1967, whose accuracy
70 is relatively low (Becker et al., 2009).

71 Satellite altimetry is a space measurement technology that uses artificial satellites
72 as a carrier to measure the distance of the satellite from the surface of the earth using
73 radar, laser, and other ranging technologies, to obtain the surface terrain of the earth,
74 through which a gravity field model and terrain features of the ocean can be constructed.
75 Parker (1972) derived the expression of gravity in the frequency domain and put
76 forward the material interface of the model of abnormal gravity changes caused by
77 fluctuations, which laid the foundation for the development of seafloor topography
78 inversion. Since the launch of the Seasat in 1978, many researchers have used satellite
79 altimetry data to model water depth, such as Dixon et al. (1983), Smith and Sandwell
80 (1994), Ramillien and Cazenave (1997), and Arabelos (1997). Calmant and Baudry
81 (1996) provided a comprehensive overview of the techniques and data used in



82 bathymetric models. Yeu et al. (2018) combined multibeam sonar, satellite altimetry-
83 derived gravity anomalies and airborne LiDAR data and managed to effectively
84 improve the accuracy of water depth measurement for up to 0.2 m in shallow waters
85 less than 5 m. Brêda et al. (2019) introduced and evaluated several data assimilation
86 (DA) methods for satellite altimetry data, which has reduced the biased bathymetry
87 errors in the hydrodynamic model for up to 65% compared to past observations while
88 at the same time increased the optimizer runtime to 103 times. Wölfl et al. (2019)
89 summarized the significance, technology, data sources, development, and challenges of
90 global seafloor topography surveys and researches and proposed recommendations for
91 the goal of a precise global bathymetry map inspired by GEBCO Seabed 2030 Project.
92 Sepúlveda et al. (2020) established a sea depth uncertainty model for satellite altimetry,
93 quantified the high-wavenumber content within the satellite-derived data and proved
94 the model in the bathymetry generated from the forecast of tsunamis, with certain
95 parameters varied regionally.

96 The emergence of satellite altimetry has made seabed topography measurement no
97 longer limited to the shipborne sonar, and has provided new technical means for large-
98 scale, real-time global measurement. However, existing researches have shown that
99 compared with the multibeam-derived bathymetry, it still has the limitation on spatial
100 resolution and thus is influenced by submarine parameters such as depth, surrounding
101 topography, computational scales and so on (Dierssen et al., 2020; Dettmering et al.,
102 2020; Wu et al., 2021).

103 In recent years, deep learning has become an important scientific computing tool
104 and made great contributions and development in various aspects such as image
105 classification (Mou et al., 2017; Li et al., 2019; Hong et al., 2021), object detection
106 (Girshick et al., 2014), feature extraction (Evans and Ruf et al., 2021), etc., making
107 multisource big data-based ocean observations available and efficient and consequently
108 being applied to the field of seafloor topography inversion. Jena et al. (2012) developed
109 an artificial neural network (ANN) model based on radial basis function (RBF) to
110 predict the water depth based on satellite-derived gravity data, with the results
111 demonstrating that the precision of the ANN model is higher than other submarine
112 topography models. Jha et al. (2013) used the geostatistical direct sampling (DS) based
113 multi-point statistics (MPS) algorithm, merging the low-frequency high-resolution
114 multibeam sonar data and high-frequency low-coverage shipborne survey data,
115 utilizing the former to provide prior constraining information to simulate and generate
116 fine depth maps. Moran (2020) discussed the global viability of machine learning
117 models for inverting bathymetry and the probability of an enhanced global model by
118 experiment and concluded machine learning could help with the determination of a
119 decision boundary when generating models. Ghorbanidehno et al. (2021) introduced a
120 principal component analysis (PCA) connected deep neural network (DNN) to perform
121 bathymetry inversion using flow velocity observations, proving its accuracy and
122 availability for a high-dimensional riverbed topography model with sparse
123 measurements.

124 By attaining the unification of the spatial resolution of multibeam data and the
125 spatial coverage of satellite altimetry data, it can provide a new means for high-



126 precision, real-time global seafloor topography surveying. In this paper, we proposed a
127 novel optimization algorithm based on VGGNet, a model for application of
128 convolutional neural network (CNN), aiming to enhance the precision of satellite
129 altimetry-derived bathymetry, which mostly lies on the range of the estimated average
130 of global ocean depth, by the input of multibeam sonar bathymetry data (Charette et al.,
131 2010).

132 The main contributions of this article are as follows.

133 1. A data combination of high-spatial-resolution multibeam sonar-derived
134 bathymetry (truth data) and high-coverage satellite altimetry-derived bathymetry (to-
135 be-corrected data) is synthesized to obtain a corrected version of the latter, with the
136 advantage from both sides.

137 2. A convolutional neural network (CNN) based VGGNet algorithm framework is
138 for the first time proposed to compute the distance (loss) between the two inputs - to-
139 be-corrected data and truth data, where the former is transformed by minimizing the
140 distance between them with backpropagation, generating an image that best match the
141 latter.

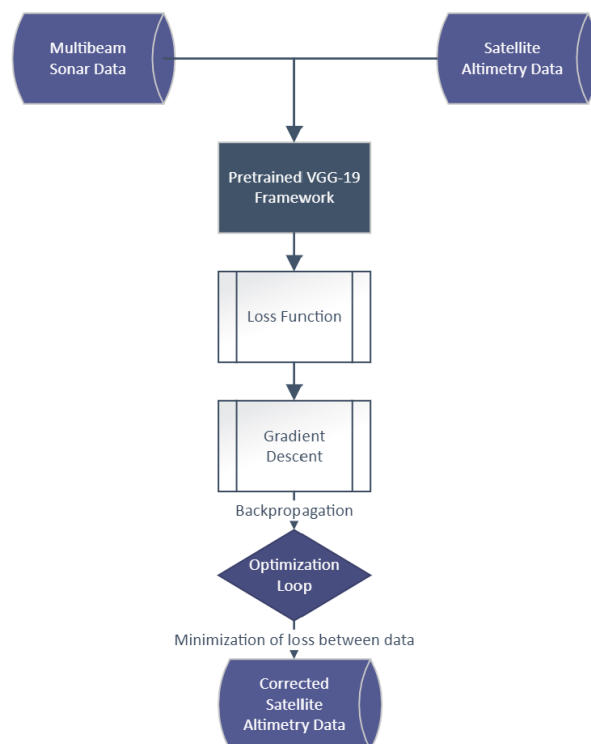
142 3. Experiments are conducted in West Pacific, Southern Ocean, and East Pacific,
143 to test the performance of the algorithm, with the results showing that the improvement
144 in computational precision can be over 17% in comparison with previous researches as
145 far as we conclude.

146
147 The rest of the article is organized as follows. An introduction to the background
148 of VGG-19 framework and the methodology of the correction of satellite altimetry-
149 derived bathymetry data using multibeam sonar data is elaborated in Section II. The
150 neural network experiments and their results are presented in Section III. Finally,
151 Section IV concludes the article.

152

153 **2 Proposed Methodology**

154 In this section, we elaborate the related background of the CNN-based VGGNet
155 (VGG-19) algorithm and its detailed application to the correction of the bathymetry
156 data. As shown in Figure 1, the structure of the proposed network consists of mainly
157 three parts: 1) the input of the truth and to-be-corrected bathymetry data; 2) the
158 designation of network model, requiring a pretrained VGG-19 framework, a loss
159 function, gradient descent, and the optimization loop; 3) the output of the corrected
160 version of satellite altimetry-derived bathymetry data.



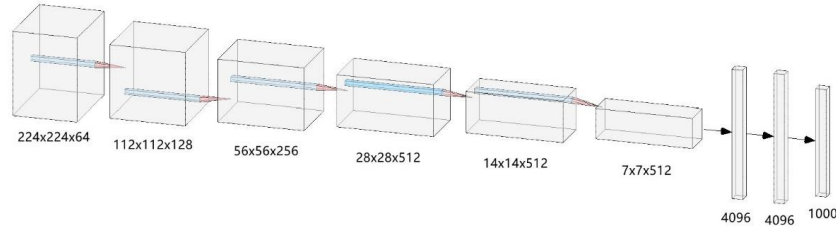
161
162
163
164
165
166
167
168
169
170
171
172
173
174
175
176
177
178
179
180
181
182

Fig.1 Main structure of the proposed network.

2.1 Framework of VGG-19

The convolutional neural network (CNN) models have been improved and updated for better application of large-scale image recognition, such as AlexNet (Krizhevsky et al., 2012), CaffeNet (Jia et al., 2014), LeNet (LeCun et al., 1998) and VGGNet (Simonyan et al., 2014), etc. Compared with most previous CNN-originated models that have 4 – 7 layers, VGG-19, a form of VGGNet, is constructed by 19 layers, which includes 16 convolutional layers and 3 fully connected layers, enabling it to extract the more abstract and deeper image features and reduce the amount of parameters while still retain the same receptive field, thus has improved the efficiency and accuracy of image computing (Huo et al., 2020; Islam et al., 2020; Schulz et al., 2020).

The structure of VGG-19 is displayed in Figure 2. The entire network uses the same size of convolution kernels (3x3) and maximum pooling kernels (2x2). The combination of several small filter (3x3) convolutional layers is better than a large one (5x5 or 7x7) in the previous models. Since the convolution kernel focuses on expanding the number of channels and the pooling kernel focuses on reducing the width and height, the architecture is deeper and wider while the increase of calculation slows down, showing the network a larger receptive field. At the same time, the network parameters are reduced, and the ReLU (Rectified Linear Unit) activation function is used multiple times to create more linear transformations to enhance the learning ability⁴⁰.



183
 184 Fig. 2 Architecture of VGGNet model used in this paper. The boxes represent the size of each
 185 layer.
 186

187 2.2 Model Training Steps

188 The correction of the bathymetry is conducted under the model of VGG-19. The
 189 principle of the correction model is to define a distance function that describes how
 190 different the two input images are. The multibeam-derived data image and the satellite
 191 altimetry-derived data image covering the same area are passed to the model, which is
 192 supposed to return the intermediate layer outputs from the model. The distance function
 193 L that we use is shown below:

$$194 \quad L^l(x, p) = \sum_{i,j} \left(F_{ij}^l(x) - P_{ij}^l(p) \right)^2 \quad (1)$$

195 where x stands for the multibeam sonar-derived bathymetry image, p stands for
 196 the satellite altimetry-derived bathymetry image, and i, j stand for the serial number
 197 of pixel points of the input images. Let V_{nn} be a pre-trained VGG-19 network and X
 198 be any image, then $V_{nn}(X)$ is the network fed by X . Let $F_{ij}^l(x) \in V_{nn}(x)$ and $P_{ij}^l(p)$

199 $\in V_{nn}(p)$ describe the respective intermediate feature representation of the network
 200 with the inputs x and p at layer l . At last, optimizers update rules are applied to
 201 iteratively update the images, which minimize a given loss with respect to the inputs.

202 The evaluation of the precision of correction is based on the comparisons with
 203 previous study. In order to quantify the differences and connections between the
 204 predicted value and truth value, here we choose two evaluation measurement, root mean
 205 square error (RMSE), normalized RMSE (NRMSE), and coefficient of determination
 206 (R^2), as follows respectively:
 207

$$208 \quad RMSE = \sqrt{\frac{\sum_{i=1}^n (\hat{f}_i - y_i)^2}{n}} \quad (2)$$

$$209 \quad NRMSE = \frac{RMSE}{y_{max} - y_{min}} \quad (3)$$



211

$$R^2 = 1 - \frac{\sum_{i=1}^n (y_i - f_i)^2}{\sum_{i=1}^n (y_i - \bar{y})^2} \quad (4)$$

213

214 where n represents the number of the values from dataset, i represents the serial
215 number of the value from the dataset, f represents the predicted values and y
216 represents the truth values. The normalization of RMSE can make data sets of different
217 numerical ranges easier to compare. $NRMSE$ and R^2 normally range from 0 – 1. The
218 smaller $RMSE$, $NRMSE$ and the bigger R^2 mean the higher correlation between the
219 datasets.

220 Using the multibeam-derived data as the content image to match, we input and
221 transformed the satellite altimetry-derived data under the framework of VGG-19 to
222 minimize the losses and distances between them so that we could attain an improved
223 bathymetry data that combined the advantages of both – the high spatial precision of
224 multibeam data and the wide spatial coverage of satellite data.

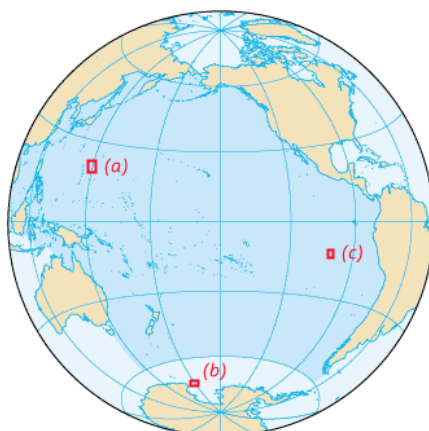
225 3 Experiments and Results

226 3.1 Experiment Data

227 The original shipborne multibeam sonar bathymetry data used in the experiment is
228 acquired at NOAA National Geophysical Data Center (2009). The interpolation
229 preprocessing on the raw data is carried out to output the gridded digital elevation model
230 (DBM) data. Meanwhile, the satellite altimetry data used in the experiment is acquired
231 and extracted from NGDC's ETOPO1 1 arc-minute global relief model, clipped with
232 the same range as that of the multibeam sonar data above (NOAA National Geophysical
233 Data Center, 2004). The grid resampling of the satellite altimetry data is performed
234 according to the resolution of the corresponding multibeam data, in order to unify the
235 resolutions of the pairs to facilitate subsequent operations.

236 We use a total of three pairs of multibeam-satellite bathymetry data respectively
237 from the West Pacific, Southern Ocean, and East Pacific, and conduct experimental
238 analysis. The location and parameters of the data are shown in Figure 3 and Table 1.

239 For the VGG-19 model, the input parameter is a pair of multibeam-satellite
240 bathymetry data, and the output parameter is the corrected satellite altimetry data. In
241 the dataset, 50% of them are randomly selected as the training set to initially fit the
242 model and update the parameters, and the remaining 50% are created as the validation
243 set to provide an unbiased evaluation of the model fitted on the training set, which is
244 the prediction results.



245
246
247
248
249

Fig. 3 Location of the bathymetry data in (a) West Pacific, (b) Southern Ocean, and (c) East Pacific.

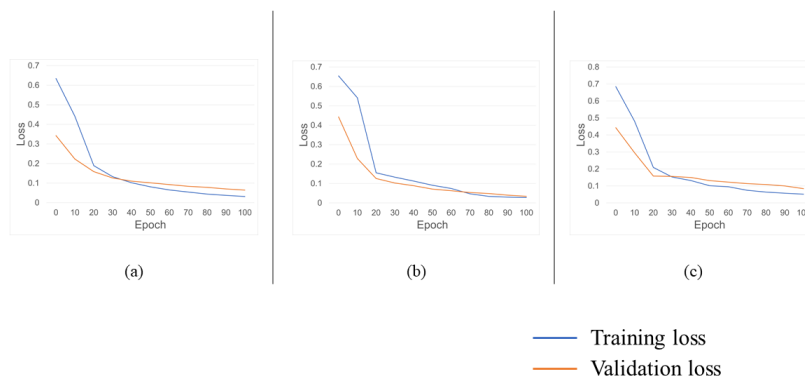
Table 1 The parameters of bathymetry data.

	Grid resolution (m)	Dataset size	Area (km²)	Depth range (m)
West Pacific	103	12,624,868	133,937	-8,987 – -369
Southern Ocean	93	5,097,104	43,700	-4,077 – -211
East Pacific	93	9,135,007	78,318	-3,921 – -1,266

250
251
252
253
254
255
256
257

3.2 Analysis of Results

The output of the deep learning model is the corrected satellite altimetry bathymetry data. Under the processing of the VGG-19 model, the surface texture of the satellite altimetry-derived seabed topography from West Pacific, Southern Ocean and East Pacific has been refined, and the water depth range has been corrected, resulting in a reduction in the distance from the truth value.



258

259

Fig.4 The loss of the training set and validation set from the model of (a) West Pacific, (b)

260

Southern Ocean and (c) East Pacific.

261

262

263

264

265

266

267

268

269

270

271

272

273

274

275

276

277

278

279

280

281

282

283

The loss function is used to estimate the gap between the output value of the model and the truth value to guide the subsequent optimization steps of the model. The smaller the loss function value, the better the model. The loss on training and test sets are shown in Figure 4. In the three experimental areas, the loss of the model has dropped sharply to around 0.2 after 20 epochs, and starts to decrease gradually, especially after 70 epochs. Moreover, it shows that no obvious overfitting phenomenon is found during the computing process. It can be concluded that the machine learning of the VGG-19 model can effectively reduce the loss for the experimental data from the three sea areas.

The parameters of the performance of the model are evaluated by running tests on 50% of the multibeam sonar data from validation set, with its outcome listed in Table 2. From the perspective of R^2 , there is a high correlation between the corrected datasets from the West Pacific, Southern Ocean and East Pacific, respectively 0.80, 0.81 and 0.77, and the truth datasets, indicating an excellent fit. In terms of RMSE and NRMSE, the figures show that the correction algorithm results in errors of 267 meters, 102 meters, and 87 meters in the Western Pacific, Southern Ocean, and Eastern Pacific datasets, along with NRMSE being 0.031, 0.026, and 0.033, respectively. Compared with previous similar studies [26] [29], our algorithm is able to improve the NRMSE of the datasets by more than 19%, proving its potential. In addition, there is a consistent trend in the changes of R^2 and RMSE, with the correction effect of the data in Southern Ocean is the best, followed by the West Pacific, and then the East Pacific.

Table 2 The precision of satellite altimetry correction.

	R^2	RMSE (m)	NRMSE
West Pacific	0.80	267	0.031
Southern Ocean	0.81	102	0.026

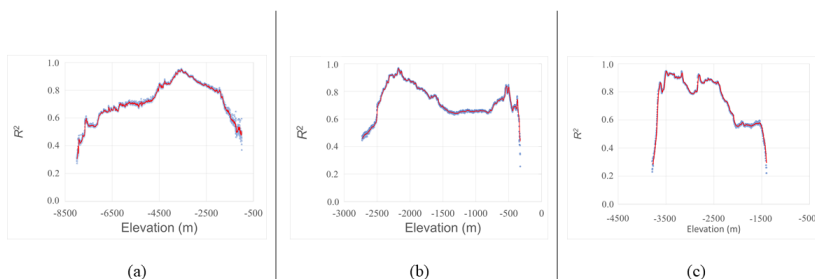


East Pacific	0.77	87	0.033
---------------------	------	----	-------

284

285 In experiments, we find that the precision of correction, taking R^2 as an example,
 286 varies with water depth, as shown in Figure 5. As can be seen from the figure, in general,
 287 the minimum of R^2 is above 0.2, which occurs at the extreme value of water depth,
 288 while the maximum can reach more than 0.9 and the water depth in each water area
 289 varies, with maximum and minimum values for each sea area being almost identical. In
 290 the West Pacific data, R^2 is higher than 0.8 in the water depth range of about -4,500 to
 291 -1,900 meters, showing a strong correlation, with a maximum at about -3,200 meters.
 292 For the Southern Ocean data, R^2 is strongly correlated at around -500 m and around -
 293 1,800 m to -2,400 m, with a maximum around -2,200 m. For the eastern Pacific data,
 294 R^2 is strongly correlated in the range of about -2,400m to -3,600m, with a maximum
 295 around -3,500m.

296 According to experiences, the precision of machine learning is positively correlated
 297 with the volume of data in the samples from dataset. Without considering other
 298 parameters, the larger the sample size, the higher the learning precision tends to be, and
 299 vice versa. In this experiment, this theory has also been verified. Combined with the
 300 histogram of water depth values, the depths where the distribution of bathymetry data
 301 points are scattered and the variance is large are often the areas where R^2 shows a low
 302 level, and the depths with high R^2 often also have more concentrated distribution and
 303 small variance. Specifically, at the maximum and minimum values of the water depths
 304 in these three sea areas, due to the small amount of sample data, the precision of
 305 machine learning is also low. Precision in the depth range where the largest sample size
 306 is distributed is highly correlated. The rise and fall of the R^2 value curves in the figure
 307 at certain water depths also reflect the particularity of the distribution of the bathymetry
 308 values of the local seabed topography to a certain extent. Experiments show that with
 309 the input of sufficient data volume, the satellite altimetry-derived bathymetry data
 310 corrected by the VGG-19 model can be highly fitted with the multibeam-derived data
 311 in specific water depth ranges.



• Bathymetry points
 — 10 meter moving average

312

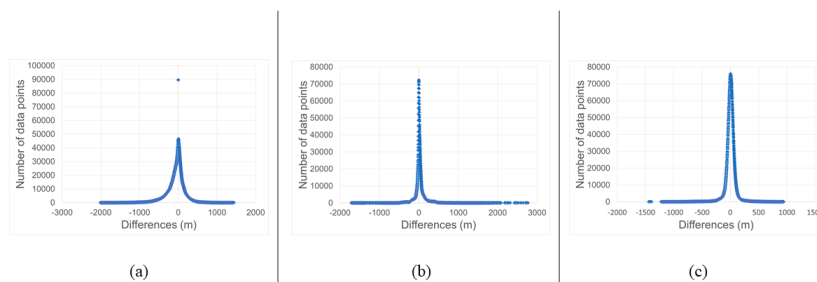


313 Fig.5 Relationship between water depth and precision (R^2) in (a) West Pacific, (b) Southern Ocean
314 and (c) East Pacific.
315

316 We subtract the corrected water depth value of satellite altimetry data from the truth
317 value of multibeam sonar data and find that the distribution of errors between the two
318 is in the form of high in the middle (zero) and low on both sides, that is, the closer the
319 error is to 0, the greater the number of data points, and vice versa, as shown in Figure
320 6. In the West Pacific data, the data point with zero error as the maximum value is
321 isolated, not continuous with the rest of the curve, indicating that the algorithm results
322 in significantly more error-free bathymetry points. In the other two data, the data curves
323 are relatively continuous, decreasing from the maximum value of zero to both sides,
324 while the curve of the Southern Ocean data is more convergent near zero than the East
325 Pacific one, indicating that its correction effect is better.

326 For a more intuitive representation, we use the absolute value of the results above
327 to calculate the percentage of the data within the range of 2%, 1% and 0.5% to the total
328 depth of each data, with the values representing the errors from the truth value, as listed
329 in Table 3. As the error range decreases, the number of data points increases gradually.
330 On average, the data points with an error within the range of 2% of the depth value
331 account for 70.58% of the total, 49.21% within the 1% range, and 30.01% within the
332 0.5% range. Compared with previous studies, the correction precision of the deep
333 learning VGG-19 model can be effectively improved by over 17%.

334 Among the depth range indicators, the accuracy of the corrected Southern Ocean
335 data is consistently better than the other two by a relatively large margin. In the 2%
336 range, the East Pacific and West Pacific data performed almost indistinguishably, with
337 the East Pacific data slightly higher. Under the strictest standard of 0.5% range, the
338 performance results of the two are widened, with the West Pacific data being better.
339 Combined with Table 2, it can be found that the changes of the parameters in the two
340 tables show relative consistency, with the data of the Southern Ocean having the best
341 correction effect, while the data of the West Pacific and East Pacific being the second
342 and lowest respectively in most cases.



◆ Bathymetry points

343

344 Fig.6 Differences between corrected and truth values in (a) West Pacific, (b) Southern Ocean and
 345 (c) East Pacific.

346

347 Table 3 Proportion of corrected errors from truth values within 2%, 1% and 0.5% depth range.

	2% of depth (%)	1% of depth (%)
West Pacific	67.25	45.73
Southern Ocean	76.19	60.34
East Pacific	68.30	41.55

348

349 4 Conclusions

350 In this study, we propose a deep learning-based VGGNet pretrained algorithm
 351 model to correct the satellite altimetry-derived bathymetry data with multibeam sonar-
 352 derived bathymetry as truth data. The core idea of the correction model is to define and
 353 minimize the distance (loss) between the truth data and the data to be corrected and
 354 finally output the corrected satellite altimetry seafloor topography accordingly. We then
 355 evaluate the model performance using three pairs of bathymetric data from the West
 356 Pacific, Southern Ocean, and East Pacific. In the process of testing, the loss of training
 357 set and validation set of the data has been effectively reduced, which proves the
 358 effectiveness of the model.

359 We selected three indicators, R^2 , RMSE and its derived NRMSE to evaluate the
 360 correction results of the data, showing excellent outcomes and the NRMSE indicator
 361 being over 19% higher than previous research. Further, by analyzing the difference of
 362 R^2 values at different water depths, we find that the correction precision of deep learning
 363 has a positive correlation trend with the sample size, that is, the accuracy of the depth
 364 values with more data points is higher, and vice versa. Finally, after finding that the
 365 difference between the truth value and the corrected value gradually decreases from the



366 maximum value at zero to both sides of the number axis, we analyze the proportion of
367 the absolute value of the difference to the overall water depth and find that our model
368 can improve the correction precision by more than 17% comparing with previous
369 research. Overall, among the three test areas, the Southern Ocean data has the highest
370 correction precision, followed by the West Pacific data, and the East Pacific data ranked
371 last.

372

373 *Code Availability.* The raw code and part of the demonstration data of the model
374 involved in this research have been archived at <https://doi.org/10.5281/zenodo.6769649>
375 (Chen et al., 2022).

376 *Author contributions.* XC and XL, ZW conceived the research. XC carried out the
377 experiments and led the writing of the paper. XQ offered guidance to the modeling
378 process. JS, MW and HW provided datasets for the experiment.

379 *Competing interests.* The contact author has declared that neither he nor their co-authors
380 have any competing interests.

381 *Acknowledgements.* This research is funded by the following project: 1) National
382 Natural Science Foundation of China (41830540). 2) National Key Research and
383 Development Program of China (2020YFC1521700 and 2020YFC1521705). 3) The
384 Open Fund of the East China Coastal Field Scientific Observation and Research Station
385 of the Ministry of Natural Resources (ORSECCZ2022104). 4) The Deep Blue Project
386 of Shanghai Jiao Tong University (SL2020ZD204). 5) Independent Project of SOED
387 State Key Laboratory of the Second Institute of Oceanography, Ministry of Natural
388 Resources (SOEDZZ2101). 6) Zhejiang Provincial Project (330000210130313013006).
389 We express our most sincere gratitude to the above funds that enable our research.

390 **References**

- 391 Amante, C., and Eakins, B. W.: ETOPO1 1 Arc-Minute Global Relief Model, NOAA
392 National Geophysical Data Center, <https://doi.org/10.7289/V5C8276M>, 2009.
- 393 Arabelos, D.: On The Possibility to Estimate Ocean Bottom Topography from Marine
394 Gravity and Satellite Altimeter Data Using Collocation, in: Geodesy on the Move,
395 edited by: Forsberg, R., Feissel, M., and Dietrich, R., Springer-Verlag, Berlin,
396 Heidelberg, Germany, 105-112, https://doi.org/10.1007/978-3-642-72245-5_13,
397 1998.
- 398 Becker, J. J., Sandwell, D. T., Smith, W. H. F., Braud, J., Binder, J., Depner, J., Fabre,
399 D., Factor, J., Ingalls, S., Kim, S.-H., Ladner, R., Marks, K., Nelson, S., Pharaoh,
400 A., Trimmer, R., Von Rosenberg, J., Wallace, G., and Weatherall, P.: Global
401 Bathymetry and Elevation Data at 30 Arc Seconds Resolution: SRTM30_PLUS,
402 Mar. Geod., 32, 355-371, <https://doi.org/10.1080/01490410903297766>, 2009.



- 403 Brêda, J. P. L. F., Paiva, R. C. D., Bravo, J. M., Passaia, O. A., Moreira, D. M.:
404 Assimilation of Satellite Altimetry Data for Effective River Bathymetry, *Water*
405 *Resour. Res.*, 55, 7441-7463, <https://doi.org/10.1029/2018WR024010>, 2019.
- 406 Calmant, S., and Baudry, N.: Modelling bathymetry by inverting satellite altimetry data:
407 A review, *Mar. Geophys. Res.*, 18, 123-134, <https://doi.org/10.1007/BF00286073>,
408 1996.
- 409 Charette, M. A., and Smith W. H. F.: The Volume of Earth's Ocean, in: *Oceanography*,
410 *Oceanography Society, Rockville, Maryland, USA*, 112-114,
411 <https://www.jstor.org/stable/24860721>, 2010.
- 412 Chen, X., Luo, X., Wu, Z., Qin, X., Shang, J., Wang, M., and Wan, H.: VGGNet-based
413 Bathymetry Correction, Zenodo [code], <https://doi.org/10.5281/zenodo.6769649>,
414 2022.
- 415 Cooper, I., Hotchkiss, R. H., and Williams, G. P.: Extending Multi-Beam Sonar with
416 Structure from Motion Data of Shorelines for Complete Pool Bathymetry of
417 Reservoirs, *Remote Sens.*, 2021, 13-35, <https://doi.org/10.3390/rs13010035>, 2021.
- 418 Dettmering, D., Ellenbeck, L., Scherer, D., Schwatke, C., and Niemann, C.: Potential
419 and Limitations of Satellite Altimetry Constellations for Monitoring Surface Water
420 Storage Changes—A Case Study in the Mississippi Basin, *Remote Sens.*, 12, 3320,
421 <https://doi.org/10.3390/rs12203320>, 2020.
- 422 Dierssen, H. M., and Theberge, A. E.: Bathymetry: Assessment, in: *Coastal and Marine*
423 *Environments*, CRC Press, Boca Raton, Florida, USA, 175-184,
424 <http://dx.doi.org/10.1201/9780429441004-19>, 2020.
- 425 Dixon, T. H., Naraghi, M., McNutt, M. K., and Smith, S. M.: Bathymetric prediction
426 from Seasat altimeter data, *J. Geophys. Res. Oceans*, 88, 1563-1571,
427 <https://doi.org/10.1029/JC088iC03p01563>, 1983.
- 428 Evans, M. C., and Ruf, C. S.: Toward the Detection and Imaging of Ocean Microplastics
429 With a Spaceborne Radar, *IEEE Trans. Geosci. Remote Sens.*, 60, 1-9,
430 <https://doi.org/10.1109/TGRS.2021.3081691>, 2022.
- 431 Fox, C. G., Chadwick Jr, W. W., and Embley, R. W.: Detection of changes in ridge -
432 crest morphology using repeated multibeam sonar surveys, *J. Geophys. Res. Solid*
433 *Earth*, 97, 11149-11162, <https://doi.org/10.1029/92JB00601>, 1992.
- 434 Ghorbanidehno, H., Lee, J., Farthing, M., Tyler, H., Darve, E. F., and Kitanidis, P. K.:
435 Deep learning technique for fast inference of large-scale riverine bathymetry, *Adv.*
436 *Water Resour.*, 147, 103715, <https://doi.org/10.1016/j.advwatres.2020.103715>,
437 2021.
- 438 Girshick, R., Donahue, J., Darrell, T., and Malik, J.: Rich Feature Hierarchies for
439 Accurate Object Detection and Semantic Segmentation, in: *Proceedings of the*
440 *27th IEEE Conference, Computer Vision and Pattern Recognition (CVPR)*,
441 *Columbus, Ohio, USA, 24-27 June 2014*, 580-587, 2014.
- 442 Hong, D., Gao, L., Yao, J., Zhang, B., Plaza, A., and Chanussot, J.: Graph Convolutional
443 Networks for Hyperspectral Image Classification, *IEEE Trans. Geosci. Remote*
444 *Sens.*, 59, 5966-5978, <https://doi.org/10.1109/TGRS.2020.3015157>, 2021.
- 445 Huo, G., Wu, Z., and Li, J.: Underwater Object Classification in Sidescan Sonar Images
446 Using Deep Transfer Learning and Semisynthetic Training Data, *IEEE access*, 8,



- 447 47407-47418, <https://doi.org/10.1109/ACCESS.2020.2978880>, 2020.
- 448 Islam, M. J., Xia, Y., and Sattar, J.: Fast Underwater Image Enhancement for Improved
449 Visual Perception, *IEEE Robot. Autom. Lett.*, 5, 3227-3234,
450 <https://doi.org/10.1109/LRA.2020.2974710>, 2020.
- 451 Jena, B., Kurian, P. J., Swain, D., Tyagi, A., and Ravindra, R.: Prediction of bathymetry
452 from satellite altimeter based gravity in the Arabian Sea: Mapping of two unnamed
453 deep seamounts, *Int. J. Appl. Earth Obs. Geoinf.*, 16, 1-4,
454 <https://doi.org/10.1016/j.jag.2011.11.008>, 2012.
- 455 Jha, S. K., Mariethoz, G., and Kelly, B. F. J.: Bathymetry fusion using multiple-point
456 geostatistics: Novelty and challenges in representing non-stationary bedforms,
457 *Environ. Model. Softw.*, 50, 66-76, <https://doi.org/10.1016/j.envsoft.2013.09.001>,
458 2013.
- 459 Ji, X.: Classification of seabed sediment and terrain complexity based on multibeam
460 data, M.S. thesis, The First Institute of Oceanography of the Ministry of Natural
461 Resources, China, 103 pp., 2017.
- 462 Jia, Y., Shelhamer, E., Donahue, J., Karayev, S., Long, J., Girshick, R., Guadarrama, S.,
463 and Darrell T.: Caffe: Convolutional Architecture for Fast Feature Embedding, in:
464 Proceedings of the 22nd ACM international conference, Multimedia, Orlando,
465 Florida, USA, 3-7 November 2014, 675-678,
466 <https://doi.org/10.1145/2647868.2654889>, 2014.
- 467 Krizhevsky, A., Sutskever, I., and Hinton, G. E.: ImageNet Classification with Deep
468 Convolutional Neural Networks, in: Advances in Neural Information Processing
469 Systems 25 (NIPS 2012), Red Hook, New York, USA, 1097-1105, 2012.
- 470 Lecun, Y., Bottou, L., Bengio, Y., and Haffner, P.: Gradient-based learning applied to
471 document recognition, *Proc. IEEE*, 86, 2278-2324,
472 <https://doi.org/10.1109/5.726791>, 1998.
- 473 Li, J.: Multibeam Survey Principles, Techniques and Methods, Ocean Press, Beijing,
474 China, 1999.
- 475 Li, S., Song, W., Fang, L., Chen, Y., Ghamisi, P., and Benediktsson, J. A.: Deep
476 Learning for Hyperspectral Image Classification: An Overview, *IEEE Trans.*
477 *Geosci. Remote Sens.*, 57, 6690-6709,
478 <https://doi.org/10.1109/TGRS.2019.2907932>, 2019.
- 479 Ma, J., Jin, J., and Liu, Q.: Multibeam Echosounder Versus Side Scan Object Detection
480 A Comparative Analysis, *Hydro. Surv. Charting*, 26, 10-12,
481 <http://dx.chinadoi.cn/10.3969/j.issn.1671-3044.2006.03.003>, 2006.
- 482 Parker, R. L.: The Rapid Calculation of Potential Anomalies, *Geophys. J. Int.*, 31, 447-
483 455, <https://doi.org/10.1111/j.1365-246X.1973.tb06513.x>, 1972.
- 484 Moran, N. P.: Machine Learning Model Selection for Predicting Global Bathymetry,
485 M.S. thesis, University of New Orleans, USA, 51 pp., 2020.
- 486 Mou, L., Ghamisi, P., and Zhu, X. X.: Deep Recurrent Neural Networks for
487 Hyperspectral Image Classification, *IEEE Trans. Geosci. Remote Sens.*, 55, 3639-
488 3655, <https://doi.org/10.1109/TGRS.2016.2636241>, 2017.
- 489 NOAA National Centers for Environmental Information: Multibeam Bathymetry
490 Database (MBBDB), NOAA National Centers for Environmental Information,



- 491 <https://doi.org/doi:10.7289/V56T0JNC>, 2004.
- 492 Pike, S., Traganos, D., Poursanidis, D., Williams, J., Medcalf, K., Reinartz, P., and
493 Chrysoulakis, N.: Leveraging Commercial High-Resolution Multispectral
494 Satellite and Multibeam Sonar Data to Estimate Bathymetry: The Case Study of
495 the Caribbean Sea, *Remote Sens.*, 11, 1830, <https://doi.org/10.3390/rs11151830>,
496 2019.
- 497 Ramillien, G., and Cazenave A.: Global bathymetry derived from altimeter data of the
498 ERS-1 geodetic mission, *J. Geodyn.*, 23, 129-149, [https://doi.org/10.1016/S0264-
499 3707\(96\)00026-9](https://doi.org/10.1016/S0264-3707(96)00026-9), 1997.
- 500 Schimel, A. C. G., Ierodiaconou, D., Hulands, L., and Kennedy, D. M.: Accounting for
501 uncertainty in volumes of seabed change measured with repeat multibeam sonar
502 surveys, *Cont. Shelf Res.*, 111, 52-68, <https://doi.org/10.1016/j.csr.2015.10.019>,
503 2015.
- 504 Schulz, M.-A., Yeo, B. T. T., Vogelstein, J. T., Mourao-Miranada, J., Kather, J. N.,
505 Kording, K., Richards, B., Bzdok, D.: Different scaling of linear models and deep
506 learning in UKBiobank brain images versus machine-learning datasets, *Nat.*
507 *Commun.*, 11, 4238, <https://doi.org/10.1038/s41467-020-18037-z>, 2020.
- 508 Sepúlveda, I., Tozer, B., Haase, J. S., Liu, P. L.-F., and Grigoriu, M.: Modeling
509 Uncertainties of Bathymetry Predicted With Satellite Altimetry Data and
510 Application to Tsunami Hazard Assessments, *J. Geophys. Res. Solid Earth*, 125,
511 e2020JB019735, <https://doi.org/10.1029/2020JB019735>, 2020.
- 512 Simonyan, K., and Zisserman, A.: Very Deep Convolutional Networks for Large-Scale
513 Image Recognition, arXiv [preprint], [arXiv:1409.1556](https://arxiv.org/abs/1409.1556), 4 September 2014.
- 514 Smith, W. H. F., and Sandwell, D. T.: Bathymetric prediction from dense satellite
515 altimetry and sparse shipboard bathymetry, *J. Geophys. Res. Solid Earth*, 99,
516 21803-21824, <https://doi.org/10.1029/94JB00988>, 1994.
- 517 Wöfl, A.-C., Snaith, H., Amirebrahimi, S., Devey, C. W., Dorschel, B., Ferrini, V.,
518 Huvenne, V. A. I., Jakobsson, M., Jencks, J., Johnston, G., Lamarche, G., Mayer,
519 L., Millar, D., Pedersen, T. H., Picard, K., Reitz, A., Schmitt, T., Visbeck, M.,
520 Weatherall, P., and Wigley, R.: Seafloor Mapping – The Challenge of a Truly
521 Global Ocean Bathymetry, *Front. Mar. Sci.*, 6, 1-16,
522 <https://doi.org/10.3389/fmars.2019.00283>, 2019.
- 523 Wu, Y.: A study on multi-beam sounding system seafloor tracking & data processing
524 techniques, Ph.D. thesis, Harbin Engineering University, China, 136 pp., 2001.
- 525 Wu, Z., Yang, F., and Tang, Y.: High-resolution seafloor survey and applications,
526 Science Press, Beijing, China, 2021.
- 527 Yeu, Y., Yee, J.-J., Yun, H. S., and Kim, K. B.: Evaluation of the Accuracy of
528 Bathymetry on the Nearshore Coastlines of Western Korea from Satellite Altimetry,
529 Multi-Beam, and Airborne Bathymetric LiDAR, *Sensors*, 18, 2926,
530 <https://doi.org/10.3390/s18092926>, 2018.